MAGNETIC RESONANCE IN CHEMISTRY
Magn. Reson. Chem. **36**, S17–S28 (1998)

Two-dimensional HSQC NMR spectra obtained using a self-compensating double pulsed field gradient and processed using the filter diagonalization method†

Vladimir A. Mandelshtam, Haitao Hu and A. J. Shaka*

Chemistry Department, University of California, Irvine, California 92697-2025, USA

Received 23 December 1997; accepted 12 January 1998

ABSTRACT: New data acquisition and data processing strategies are combined to give enhanced 2D HSQC spectra. Complete carbon-13 assignments can be obtained using only two proton spectra in some cases. A composite pulsed field gradient is employed which appears effectively instantaneous, as far as spin evolution is concerned, and which offers superb recovery and does not perturb the field/frequency lock. The spectra are analyzed by a new linear algebraic method called the filter diagonalization method (FDM). FDM can be used to extract 2D spectral parameters directly from 2D time signals without any Fourier transformation and can speed up the spectral throughput. © 1998 John Wiley & Sons, Ltd.

KEYWORDS: HSQC; gradients; filter diagonalization

INTRODUCTION

Time, either instrument time or computer time, is money. In two-dimensional (2D) NMR spectra one may not be able to afford the luxury of acquiring a sufficiently long signal to obtain the desired resolution in the interferometric (F_1) dimension because each t_1 increment requires at least one repetition of the entire pulse sequence including an appropriate relaxation delay. Long acquisition times in the F_1 dimension adversely impact the sensitivity of the 2D experiment: if the maximum acquisition time in F_1, $t_{1,\max}$, becomes long, sensitivity is markedly decreased, necessitating extensive time averaging to obtain an acceptable signal-to-noise ratio in the final spectrum.[1] Furthermore, in many cases one has a phase-modulated data set, obtained naturally by coherence transfer pathway selection[2] using pulsed field gradients[3,4] (PFGs), but has to repeat each scan with the polarity of one of the gradient pulses reversed so that 'N-' and 'P-type' data sets can be obtained. These are then combined, after Fourier transformation with respect to the running time t_2, to give the usual amplitude-modulated data sets from which a phase-sensitive double absorption lineshape can be obtained.[5] It is well known that spectra which are purely phase modulated as a function of t_1 give rise to mixed-phase ('phase-twist') lineshapes in which neither the real nor imaginary part of the 2D Fourier transform (FT) spectrum can be phased to the desired double absorption lineshape.[6] This phenomenon is unavoidable in homonuclear 2D *J*-resolved spectroscopy,[7] in which the phase-twist lineshape both distorts proton multiplet cross-sections and necessitates an absolute-value 45° integral projection when trying to obtain a homonuclear decoupled proton spectrum, leading to disappointing resolution in the decoupled spectrum.

The origin of the phase-twist lineshape can be understood by considering the FT of a normalized one-dimensional time signal:

$$C(t) = \exp(i\varphi)\exp(i2\pi ft)\exp(-\gamma t) \tag{1}$$

which gives the spectrum

$$S(F) = \exp(i\varphi)\left(\frac{\gamma}{\gamma^2 + 4\pi^2(F-f)^2} + i\,\frac{2\pi(F-f)}{\gamma^2 + 4\pi^2(F-f)^2}\right)$$
$$\equiv \exp(i\varphi)[A(F-f) + iD(F-f)] \tag{2}$$

where A and D are the absorption and dispersion Lorentzian lineshape functions, respectively. It is thus possible to choose the overall phase φ so that the real part of the FT spectrum contains only the absorption-mode lineshape; with a many-line spectrum the same holds provided that φ is a known function of frequency that does not vary too much across the width of a typical line. In the analogous 2D case, however,

$$C(t_1, t_2) = \exp(i\varphi)\exp(i2\pi f_1 t_1)\exp(-\gamma_1 t_1)$$
$$\times \exp(i2\pi f_2 t_2)\exp(-\gamma_2 t_2) \tag{3}$$

we find

$$S(F_1, F_2) = \exp(i\varphi)[A_1(F_1 - f_1) + iD_1(F_1 - f_1)]$$
$$\times [A_2(F_2 - f_2) + iD_2(F_2 - f_2)] \tag{4}$$

* Correspondence to: A. J. Shaka, Chemistry Department, University of California, Irvine, California 92697-2025, USA.
E-mail: ajshaka@uci.edu
† Dedicated to Professor John D. Roberts on the occasion of his 80th birthday.
Contract/grant sponsor: Dreyfus Foundation.
Contract/grant sponsor: National Science Foundation; *contract/grant number*: CHE-9625674.

CCC 0749-1581/98/SI0017–12 $17.50

showing that, even when φ is correctly chosen, the real part of the 2D spectrum has a lineshape function $A_1 A_2 - D_1 D_2$ rather than the double absorption $A_1 A_2$ lineshape. In nD purely phase-modulated spectra one can compute the real or imaginary part of $\Pi_k(A_k + iD_k)$ which, in the 3D case gives, for example, $A_1 A_2 A_3 - A_1 D_2 D_3 - D_1 A_2 D_3 - D_1 D_2 A_3$.

Additional problems in PFG versions of 2D experiments may arise due to the non-zero time it takes to apply a strong gradient pulse and the recovery delay that needs to be included after the gradient to let the field stabilize. These delays can add up to *ca.* 1 ms, during which time chemical shift evolution occurs. As a result, the phase φ becomes frequency dependent, sometimes in each dimension, making correct phasing of the spectrum problematic. These difficulties often allow only absolute value presentation of many kinds of heteronuclear PFG spectra like the popular heteronuclear single-quantum coherence (HSQC) experiment.[8]

In this paper we will outline a solution to the problems above so that absorption-like high-resolution spectra can be obtained from purely phase-modulated signals. Our approach is partly in the design of the pulse sequence and partly in the data processing. On the pulse sequence side we will introduce a 'pure' nucleus-selective PFG in which other terms in the spin Hamiltonian behave as if the PFG were instantaneous. Using this approach, the phase remains well behaved, with no linear frequency phase corrections needed. On the data processing side we outline an important new alternative method to standard FT or linear prediction (LP) analysis called the filter diagonalization method (FDM) and apply it to purely phase-modulated data sets obtained from the new PFG version of the HSQC pulse sequence. The method shares some of the features of the LP technique[9–13] but is superior computationally with regard to speed, stability, the ability to process efficiently very long time signals with many (e.g. 10^6) spectral features and direct fully integrated 2D processing. FDM produces a direct line list of the spectral features and can operate with far fewer t_1 increments than is customary, as we will demonstrate. We are thus able to acquire the data more efficiently, process them more rapidly and obtain a line list with good fidelity.

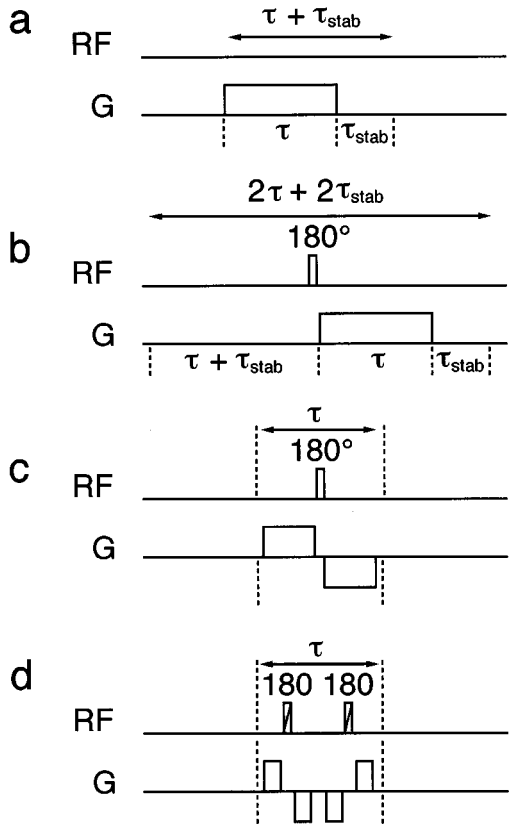

Figure 1. Four different pulsed field gradient sequences. (a) A gradient of length τ is followed by a stabilization delay τ_{stab}. Typical values might be 1 ms and 200 μs, respectively. Chemical shifts and couplings will evolve throughout this time. (b) A compensating conventional refocusing pulse can be used to compensate for the gradient time and stabilization delay. The sequence becomes twice as long and the 180° pulse can give rise to artifacts if it is imperfect. (c) The scheme proposed by Wider *et al.*[14] in which the 180° pulse is placed within the gradient and half of the gradient pulse is applied with opposite polarity. The stabilization time τ_{stab} becomes negligible with this arrangement, but suppression of unwanted transverse magnetization is imperfect. (d) The modified double echo scheme proposed in this work. Two high-power, constant-amplitude frequency-modulated pulses (shown as the scored icons), with superior inversion performance are applied between two sets of antiphase gradients with unequal strengths. Suppression of unwanted magnetization is improved, as is retention of desired signals. The poor phase properties of the 180°s have no effect on the performance because there are two of them.

SELF-COMPENSATING PULSED FIELD GRADIENTS

Figure 1 shows some timing diagrams for several combinations of radiofrequency (RF) pulses and gradients. Just as there is an accepted ideal for an inversion pulse, namely mapping $I_z \rightarrow -I_z$ independent of resonance offset or RF inhomogeneity, we need to formulate the corresponding ideal for a PFG. Our ideal PFG is an infinitely intense zero-duration gradient pulse that winds all transverse magnetization of a selected spin species into a perfect helix of specified pitch along the gradient axis with zero recovery time needed after the application of the gradient pulse, leaving z-magnetization unaffected. An instantaneous gradient allows no time for evolution under chemical shift of spin–spin coupling, the suppression ratio depends on *all* transverse magnetization being affected, the specificity is important for some realizations of 'joint' experiments and the recovery time criterion means that either data acquisition or further pulses can be applied immediately following the ideal PFG. As in the area of composite 180° pulses, we can make up for instrumental limitations such as finite gradient amplitude and non-zero recovery time by combining several PFGs with RF

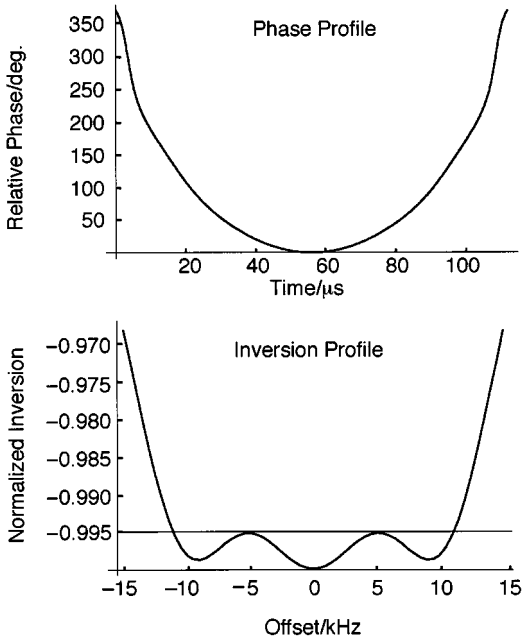

Figure 2. Phase profile versus time and inversion profile versus frequency of a constant-amplitude FM pulse. Better than 99.5% inversion is achieved over the most of the 25 kHz carbon-13 bandwidth using a 112 μs pulse with an RF field of 17.8 kHz. Better than 97% inversion is achieved over 30 kHz.

pulses. This simplest modification, Fig. 1(b) is to introduce a 180° pulse and a compensating delay. To the extent that the 180° pulse is imperfect, this scheme may lead to artifacts in the spectrum, but the suppression of transverse magnetization is still perfect. Figure 1(c) shows an improved modification introduced by Wider *et al.*[14] in which the conventional PFG is replaced by a matched antiphase pair of PFGs with a conventional 180° pulse in the center. An analysis of this sequence shows that the fraction of spins not flipped by the 180° pulse give rise to a signal which has no spatial encoding. That is, if M_z is the final expectation value of z-magnetization after the 180° pulse, starting from equilibrium $+M_0$, and the spin flip probability is defined by

$$P = \frac{1}{2}\left(1 - \frac{M_z}{M_0}\right) \tag{5}$$

then a fraction $1 - P$ of transverse magnetization 'breaks through' the sequence, with no spatial encoding. For a conventional 180° pulse this fraction can be up to 10% off-resonance depending on the available RF pulse power and the spatial inhomogeneity of the RF field over the detected sample volume, leading to very modest suppression ratios of the order of 10–50 instead of the essentially infinite ratio achieved by a conventional gradient, Fig. 1(a). For the part of the magnetization P which experiences the 180° pulse, chemical shift evolution and heteronuclear spin–spin coupling are refocused, making the sandwich appear nearly instantaneous. Homonuclear J coupling will still evolve, but in practical applications $J\tau_g \ll 1$ for proton couplings $J \approx 10$ Hz and PFG times $\tau_g \approx 1$ ms. Because the eddy currents induced by a positive polarity PFG are nearly canceled by the juxtaposed negative polarity PFG, recovery is substantially improved.[14] In addition, as no 180° pulses are applied to the deuterium lock channel, the field-frequency lock signals is only momentarily perturbed. The z-magnetization of the 'target' spins is, however, inverted by this sequence, meaning that the latter cannot represent a true ideal gradient, and causing problems in the case of a large positive H_2O z-magnetization which becomes inverted and then becomes subject to radiation damping effects.[15]

It is a simple matter to fix both the suppression of transverse magnetization and inversion of z-magnetization problems by modifying the sequence to the double inversion sequence of Fig. 1(d). In this sequence essentially any inversion pulse can be used because the use of two such pulses leads to no unwanted phase shifts where the inversion is excellent. This sequence is just a broadband version of the double pulsed field gradient spin echo (DPFGSE) sequence,[16] in which the current drive of the center pair of gradients is reversed. As such, we propose to use a broadband high-power constant-amplitude frequency-modulated (FM) pulse to achieve $P \to 1$. In addition, the 'breakthrough' expression becomes $(1 - P)^2$, which is much less than $1 - P$ when $P \to 1$. In practice, suppression ratios of several hundred are obtained.[17] Finally, z-magnetization is restored ($I_z \to +I_z$). One advantage of our approach is that the modified gradient can be directly substituted for a conventional gradient in any pulse sequence, as it transforms magnetization equivalently.

For HSQC applications, the 180° pulse may have to invert the entire carbon-13 bandwidth of *ca.* 25 kHz on a 500 MHz spectrometer. The maximum convenient RF field we can achieve on carbon-13 is 17.8 kHz, or about a 14 μs 90° time. We therefore set out to find a suitably brief and accurate high-power FM pulse for this application. Good results were obtained with the pulse shown in Fig. 2. The 112 μs duration of this constant-amplitude broadband inversion pulse is relatively brief, and the extent of inversion is better than 99.5% over the entire protonated carbon-13 chemical shift range. There is also a high tolerance for pulse miscalibration or RF inhomogeneity. This highly efficient FM pulse has a nominal length of 720°, eight times the length of a 90° pulse; parameters for the pulse are given in Table 1. This family of inversion pulses, which are related to the modulated inversion pulses described by Baum *et al.*,[18] will be described more fully elsewhere.

THE FILTER DIAGONALIZATION METHOD (FDM)

FDM was first introduced in 1995 by Wall and Neuhauser[19] as a method of spectral analysis of time correlation functions in quantum dynamics calculations. Recently it has been substantially improved[20,21] and

Table 1. Numerical Listing of Phase versus Time for the Broadband Inversion Pulse of Fig. 2*

t/μs	φ/deg.	t/μs	φ/deg.	t/μs	φ/deg.	t/μs	φ/deg.	t/μs	φ/deg.	t/μs	φ/deg.
0.0	368.4	10.0	186.6	20.0	106.9	30.0	52.5	40.0	19.9	50.0	2.7
0.2	366.5	10.2	184.8	20.2	105.5	30.2	51.6	40.2	19.4	50.2	2.5
0.4	364.4	10.4	183.1	20.4	104.1	30.4	50.9	40.4	18.9	50.4	2.3
0.6	362.0	10.6	181.3	20.6	102.7	30.6	50.0	40.6	18.4	50.6	2.1
0.8	359.5	10.8	179.6	20.8	101.4	30.8	49.3	40.8	17.9	50.8	2.0
1.0	356.7	11.0	177.9	21.0	100.0	31.0	48.5	41.0	17.5	51.0	1.8
1.2	353.6	11.2	176.2	21.2	98.7	31.2	47.7	41.2	17.0	51.2	1.7
1.4	350.2	11.4	174.5	21.4	97.4	31.4	46.9	41.4	16.5	51.4	1.6
1.6	346.4	11.6	172.8	21.6	96.1	31.6	46.2	41.6	16.1	51.6	1.4
1.8	342.3	11.8	171.2	21.8	94.8	31.8	45.4	41.8	15.7	51.8	1.3
2.0	337.8	12.0	169.5	22.0	93.5	32.0	44.7	42.0	15.2	52.0	1.1
2.2	332.9	12.2	167.9	22.2	92.2	32.2	43.9	42.2	14.8	52.2	1.0
2.4	327.3	12.4	166.2	22.4	90.9	32.4	43.2	42.4	14.3	52.4	0.9
2.6	321.6	12.6	164.6	22.6	89.7	32.6	42.4	42.6	13.9	52.6	0.8
2.8	315.5	12.8	162.9	22.8	88.5	32.8	41.7	42.8	13.5	52.8	0.7
3.0	309.2	13.0	161.3	23.0	87.3	33.0	41.0	43.0	13.1	53.0	0.6
3.2	302.6	13.2	159.7	23.2	86.1	33.2	40.3	43.2	12.7	53.2	0.5
3.4	296.0	13.4	158.0	23.4	84.9	33.4	39.6	43.4	12.3	53.4	0.5
3.6	289.4	13.6	156.4	23.6	83.7	33.6	38.9	43.6	11.9	53.6	0.4
3.8	283.2	13.8	154.8	23.8	82.6	33.8	38.2	43.8	11.5	53.8	0.3
4.0	277.2	14.0	153.2	24.0	81.4	34.0	37.5	44.0	11.1	54.0	0.3
4.2	271.3	14.2	151.6	24.2	80.3	34.2	36.9	44.2	10.7	54.2	0.2
4.4	265.7	14.4	149.9	24.4	79.2	34.4	36.2	44.4	10.3	54.4	0.1
4.6	260.4	14.6	148.3	24.6	78.1	34.6	35.5	44.6	10.0	54.6	0.1
4.8	255.7	14.8	146.8	24.8	77.0	34.8	34.9	44.8	9.6	54.8	0.1
5.0	251.0	15.0	145.1	25.0	75.9	35.0	34.2	45.0	9.3	55.0	0.0
5.2	246.8	15.2	143.6	25.2	74.8	35.2	33.6	45.2	9.0	55.2	0.0
5.4	242.8	15.4	142.0	25.4	73.8	35.4	33.0	45.4	8.6	55.4	0.0
5.6	239.0	15.6	140.4	25.6	72.7	35.6	32.3	45.6	8.3	55.6	0.0
5.8	235.5	15.8	138.8	25.8	71.7	35.8	31.7	45.8	8.0	55.8	0.0
6.0	232.2	16.0	137.2	26.0	70.7	36.0	31.1	46.0	7.7		
6.2	229.0	16.2	135.7	26.2	69.7	36.2	3.05	46.2	7.4		
6.4	226.0	16.4	134.0	26.4	68.7	36.4	29.8	46.4	7.0		
6.6	223.1	16.6	132.5	26.6	67.7	36.6	29.2	46.6	6.7		
6.8	220.4	16.8	130.9	26.8	66.7	36.8	28.7	46.8	6.4		
7.0	217.8	17.0	129.4	27.0	65.8	37.0	28.1	47.0	6.2		
7.2	215.3	17.2	127.8	27.2	64.8	37.2	27.5	47.2	5.9		
7.4	212.8	17.4	126.3	27.4	63.9	37.4	26.9	47.4	5.6		
7.6	210.5	17.6	124.7	27.6	62.9	37.6	26.3	47.6	5.4		
7.8	208.2	17.8	123.2	27.8	62.0	37.8	25.7	47.8	5.1		
8.0	206.0	18.0	121.6	28.0	61.1	38.0	25.2	48.0	4.8		
8.2	203.9	18.2	120.1	28.2	60.2	38.2	24.6	48.2	4.6		
8.4	201.8	18.4	118.6	28.4	59.3	38.4	24.1	48.4	4.4		
8.6	199.8	18.6	117.1	28.6	58.4	38.6	23.5	48.6	4.1		
8.8	197.8	18.8	115.6	28.8	57.5	38.8	23.0	48.8	3.9		
9.0	195.8	19.0	114.1	29.0	56.7	39.0	22.5	49.0	3.7		
9.2	193.9	19.2	112.7	29.2	55.8	39.2	21.9	49.2	3.5		
9.4	192.0	19.4	111.2	29.4	55.0	39.4	21.4	49.4	3.3		
9.6	190.2	19.6	109.8	29.6	54.1	39.6	20.9	49.6	3.1		
9.8	188.4	19.8	108.3	29.8	53.3	39.8	20.4	49.8	2.9		

* The phase profile is an even function of time. Only the first half of the pulse is listed.

extended to the case of multi-dimensional time signals.[22,23] In this section we will briefly describe the basic ideas needed to apply FDM to a one-dimensional time signal; the corresponding 2D case can be found in the Appendix.

The object of FDM is to fit a given complex time signal $c_n = C(t_n)$ defined on an equidistant time grid $t_n = n\tau$, $n = 0, 1, \ldots, N-1$, to the sum of exponentially damped sinusoids:

$$c_n = \sum_{k=1}^{K} d_k \exp(-in\tau\omega_k) = \sum_{k=1}^{K} d_k \exp(-2\pi in\tau f_k) \exp(-n\tau\gamma_k) \quad (6)$$

with a total of $2K$ unknowns, the K complex amplitudes d_k and the K complex frequencies $\omega_k = 2\pi f_k - i\gamma_k$, which include damping. For brevity, we will refer to this problem as a harmonic inversion problem (HIP). The more compact notation ω_k is preferred as, in FDM, the imaginary parts γ_k (widths) of the frequencies always appear together with the real parts $2\pi f_k$ (positions).

Even though the fitting problem of Eqn (6) is highly nonlinear, its solution can be obtained by pure linear algebra. This is the essential simplification that the assumption of a Lorentzian lineshape allows. This feature is not unique to FDM and is shared by several other 'high-resolution' methods, including the Prony method, MUSIC, ESPRIT, LP, etc.[9–13,24,25] The central ansatz (assumption) of FDM is to associate the signal c_n to be fitted by the form of Eqn (6) with the time autocorrelation function of a fictitious dynamic system described by an effective complex symmetric Hamiltonian operator $\hat{\Omega}$ with eigenvalues $\{\omega_k\}$:[19]

$$c_n = (\Phi_0 \,|\, \exp(-in\tau\hat{\Omega})\Phi_0) \tag{7}$$

Here a complex symmetric inner product is used, $(a\,|\,b) = (b\,|\,a)$ without complex conjugation and Φ_0 is some 'initial state.' The problem of fitting the observed time signal to the form of Eqn (6) thus becomes equivalent to diagonalizing the Hamiltonian $\hat{\Omega}$ or, equivalently, the evolution operator[20] $\hat{U} = \exp(-i\tau\hat{\Omega})$.

Suppose that there is a set of orthonormal eigenvectors, $\{\mathcal{Y}_k\}$, that diagonalizes $\hat{\Omega}$. Then,

$$\hat{\Omega} = \sum_k \omega_k \,|\, \mathcal{Y}_k)(\mathcal{Y}_k \,|\, \tag{8}$$

is the spectral decomposition of $\hat{\Omega}$. Inserting Eqn (8) into Eqn (7), we can obtain Eqn (6) with

$$d_k = (\Phi_0 \,|\, \mathcal{Y}_k)(\mathcal{Y}_k \,|\, \Phi_0) = (\mathcal{Y}_k \,|\, \Phi_0)^2 \tag{9}$$

Note that under the assumption that $\hat{\Omega}$ has a finite rank, the LP equations can be derived from Eqn (7). However, FDM does not require $\hat{\Omega}$ to be of finite rank. In addition, FDM does not require one to assume a value for K, the *true* number of lines in the spectrum, or even that K be finite because, as will be seen below, the eigenvalues ω_k in the frequency window of interest will not be affected by the spectral propertiess of $\hat{\Omega}$ outside this window.

Even though the operator $\hat{\Omega}$ is not explicitly available, its matrix elements in an appropriately chosen basis are determined completely by the measured values c_n. Such a basis can be chosen in many different ways. For example, it was shown[20,21] that for a finite signal of length $N \approx 2M$ one can devise a suitable basis by taking a linear combination of the primitive Krylov basis functions $\Phi_n = \hat{U}^n\Phi_0$ with $n = 0, 1, \ldots, M$. It was also proposed[20] to employ a rectangular window Fourier basis:

$$\Psi(\varphi) = \sum_{n=0}^{M} \exp(in\varphi)\Phi_n \equiv \sum_{n=0}^{M} \exp[in(\varphi - \hat{\Omega}\tau)]\Phi_0 \tag{10}$$

with a set of φ values taken in a small pre-specified frequency interval (see below). This is a simpler and more efficient analog of the Gaussian window Fourier basis originally proposed by Wall and Neuhauser.[19] To recast the nonlinear fitting problem of Eqn (6) as a linear algebraic problem, we only have to show that the matrix elements of the operator $\hat{U}^p = \exp(-ip\tau\hat{\Omega})$ between any two functions $\Psi(\varphi)$ and $\Psi(\varphi')$, defined by Eqn (10), can be evaluated only in terms of the measured signal c_n. This can be shown using the ansatz of Eqn (7):

$$\begin{aligned} U^{(p)}(\varphi', \varphi) &\equiv (\Psi(\varphi')|\, \hat{U}^p\Psi(\varphi)) \\ &= \sum_{n'=0}^{M}\sum_{n=0}^{M} \exp(in\varphi)\exp(in'\varphi') \\ &\quad \times \{\exp(-in'\tau\hat{\Omega})\Phi_0 \,|\, \exp[-i(n+p)\tau\hat{\Omega}]\Phi_0\} \\ &= \sum_{n'=0}^{M}\sum_{n=0}^{M} \exp[in(\varphi - \varphi')] \\ &\quad \times \exp[i(n+n')\varphi']c_{n+n'+p} \end{aligned} \tag{11}$$

Since the basis $\{\Psi(\varphi)\}$ is not orthonormal, we will also need the overlap matrix $(\Psi(\varphi)|\,\Psi(\varphi'))$, which corresponds to $p = 0$.

A Fourier basis is probably the most important aspect of FDM that makes it numerically superior to other linear algebraic methods of solving the fitting problem of Eqn (6). The local nature of the Fourier basis allows a solution for the frequencies ω_k in a small *a priori* chosen frequency interval, which operationally involves only small matrices corresponding to a small (and only locally complete) basis $\{\Psi(\varphi_j)\}$, $j = 1, 2, \ldots, K_{\text{win}}$. This greatly reduces the numerical effort for both matrix evaluation and for solution of the resulting small generalized eigenvalue problem. Interestingly, the LP-ZOOM method, proposed by Tang and Norris[26] in 1988, theoretically shares many of the advantages of FDM for 1D spectral analysis. LP-ZOOM is a modification of the LP algorithm for local spectral analysis. It is numerically distinct from FDM, but is similar in spirit.

A detailed derivation of the version of 1D FDM that we employ can be found elsewhere.[21,22] The numerical procedure can be summarized by the following steps:

1. Choose a small enough frequency window $[f_{\min}, f_{\max}]$ for the spectral analysis of a given signal $c_n = C(t_n)$, $n = 0, 1, 2, \ldots, N-1$. 'Small enough' is operationally defined by the resulting size of the linear algebraic problem.
2. Set up an evenly spaced (if not specified otherwise) angular frequency grid $2\pi f_{\min} < \varphi_j/\tau < 2\pi f_{\max}$, $j = 1, 2, \ldots, K_{\text{win}}$, by choosing an appropriate value for K_{win}. A reasonable choice for K_{win} is $K_{\text{win}} = N(f_{\max} - f_{\min})/2SW$ where SW is the spectral width $1/\tau$. This is simply half the number of points that would appear in a conventional N-point complex Fourier transform of c_n within this same frequency window

which is consistent with the informational content of the data array c_n, i.e. this value of K_{win} is the largest number of lines that can give a unique fit to a signal of this length.

3. Evaluate three complex symmetric matrices $\mathbf{U}^{(p)}$ of the size $K_{win} \times K_{win}$ for, e.g., $p = 0, 1, 2$, using for the matrix elements of $\mathbf{U}^{(p)}_{jj'} \equiv \mathbf{U}^{(p)}(\varphi_j, \varphi_{j'})$:

$$\mathbf{U}^{(p)}(\varphi, \varphi') = \sum_{n=0}^{2M} S_n(\varphi, \varphi'; M) c_{n+p} \qquad (12)$$

with $M = (N - 2)/2$. Here, for $\varphi \neq \varphi'$, the signal-independent kernel $S_n(\varphi, \varphi'; M)$ is given by

$$\begin{aligned} S_n(\varphi, \varphi'; M) &= ([\exp(-i\varphi) \exp(-in\varphi') \\ &\quad - \exp(-i\varphi') \exp(in\varphi)] \\ &\quad \times \theta(n - M) \\ &\quad + \{\exp[iM(\varphi' - \varphi)] \exp[i(n-1)\varphi] \\ &\quad - \exp[-iM(\varphi' - \varphi)] \exp[i(n-1)\varphi']\} \\ &\quad \times [1 - \theta(n - M)] \\ &\quad / [\exp(-i\varphi) - \exp(-i\varphi')] \end{aligned} \qquad (13)$$

with $\theta(n) = 0$ if $n \leqslant 0$ and $\theta(n) = 1$ if $n > 0$; and

$$S_n(\varphi, \varphi; M) = [M + 1 - |M - n|] \exp(in\varphi) \qquad (14)$$

Equation (12) is derived from Eqn (11) by the substitution $l = n + n'$, which eliminates one of the two summations.

4. Solve the generalized eigenvalue problem

$$\mathbf{U}^{(1)}\mathbf{B}_k = u_k \mathbf{U}^{(0)}\mathbf{B}_k \qquad (15)$$

for the eigenvalues $u_k = \exp(-i\tau\omega_k)$ and eigenvectors $\mathbf{B}_k$, using, e.g., a singular value decomposition (SVD) of the matrix $\mathbf{U}^{(0)}$.

5. Accept those eigenvalues u_k which satisfy an error criterion as, e.g.,

$$\|(\mathbf{U}^{(2)} - u_k{}^2\mathbf{U}^{(0)})\mathbf{B}_k\| < \varepsilon \qquad (16)$$

for a small enough ε.

6. Go to the next step or, optionally, set up a new grid by taking $\{\varphi_k\} = \{\tau\omega_k\}$ and iterate by going to step 3.

7. Compute the complex amplitudes d_k using the expression

$$d_k^{1/2} = \sum_{j=1}^{K_{win}} B_{jk} \sum_{n=0}^{M} c_n \exp(in\varphi_j) \qquad (17)$$

or a substantially more accurate expression

$$\begin{aligned} d_k^{1/2} &= \frac{1 - \exp(-\tau\gamma)}{1 - \exp[-(M+1)\tau\gamma]} \\ &\quad \times \sum_{j=1}^{K_{win}} B_{jk} U^{(0)}[\varphi_j, \tau(\omega_k + i\gamma)] \end{aligned} \qquad (18)$$

The adjusting parameter γ is chosen so that $U^{(0)}[\varphi_j, \tau(\omega_k + i\gamma)]$ is numerically stable. One correct choice is $\gamma = -\mathrm{Im}\{\omega_k\}$ for $\mathrm{Im}\{\omega_k\} < 0$ and $\gamma = 0$ for $\mathrm{Im}\{\omega_k\} > 0$.

8. Store the set of converged ω_k and d_k and use them as input for a spectral estimator which, for the absorption mode 'ersatz' spectrum,[23] corresponds to

$$A(F) = -\sum_k \mathrm{Im}\left\{\frac{d_k}{2\pi F - \omega_k}\right\} \qquad (19)$$

If $\mathrm{Im}\{\omega_k\} > 0$ then ω_k is replaced with ω_k*.

9. Choose the next frequency window.

A few comments are in order. First, note that in FDM the complex amplitudes are computed without solving another linear least-squares problem, in contrast to all other linear algebraic approaches. Note that the formula for the amplitude and phase of each feature as given in Eqn (17) or (18) does not depend on the values of the other complex frequencies. In conventional LP methods, the amplitudes are constructed by solving a linear system which uses, as part of its input, all the obtained frequencies. In a few cases ω_k might have a positive imaginary part, resulting in a 'negative' linewidth. These 'bad' roots complicate the correct determination of the amplitudes of other features. One regularization procedure is simply to change the sign of the imaginary part. We adopt this procedure when constructing the ersatz spectrum using Eqn (19), replacing ω_k with ω_k*. Note that in FDM this replacement does not affect the other spectral features.

A general two-dimensional analog of the HIP, Eqn (6), can be formulated as a nonlinear fit of a 2D time-domain array c_{n_1,n_2} with $0 < n_1 < N_1$, and $0 < n_2 < N_2$, by the plane wave representation:

$$c_{n_1,n_2} = \sum_{k=1}^{K} d_k \exp(-in_1\tau_1\omega_{1k}) \exp(-in_2\tau_2\omega_{2k}) \qquad (20)$$

with a total $3K$ unknown complex numbers, i.e. the K complex amplitudes d_k and a set of K complex pairs of frequencies $(\omega_{1k}, \omega_{2k})$. Note that this case corresponds exactly to pure phase modulation, the situation in which the 2D FT spectrum produces phase-twist lineshapes. The analysis proceeds in a similar way as for 1D FDM, but with a two-dimensional frequency window $[f_{1\min}, f_{1\max}] \times [f_{2\min}, f_{2\max}]$.

There are a number of different ways to construct a 2D ersatz spectrum. One useful equation, in which it is expected that all the lines have the same initial phase in F_1, is simply

$$A(F_1, F_2) = \sum_k \mathrm{Im}\left\{\frac{1}{2\pi F_1 - \omega_{1k}}\right\} \mathrm{Im}\left\{\frac{d_k}{2\pi F_2 - \omega_{2k}}\right\} \qquad (21)$$

although, if the phase is well behaved, it can be simpler to employ alternative representations such as

$$\begin{aligned} A(F_1, F_2) = \sum_k |d_k| \, &\mathrm{Im}\left\{\frac{1}{2\pi F_1 - \omega_{1k}}\right\} \\ &\times \mathrm{Im}\left\{\frac{1}{2\pi F_2 - \omega_{2k}}\right\} \end{aligned} \qquad (22)$$

$$A(F_1, F_2) = \sum_k \text{Re}\{d_k\} \text{Im}\left\{\frac{1}{2\pi F_1 - \omega_{1k}}\right\} \times \text{Im}\left\{\frac{1}{2\pi F_2 - \omega_{2k}}\right\} \quad (23)$$

where the latter expression allows the correct interpretation of negative spectral features. Because FDM gives the list of spectral parameters as its output, there is some freedom in how one chooses to construct a spectral representation from them. It is always possible to construct a representation which would agree with the FT spectrum, although this is clearly not profitable if the FT spectrum consists of phase-twist lineshapes.

In some cases, FDM may allow fewer time-domain data points to be acquired. In the absence of degeneracy, all the unknown parameters d_k, ω_{1k}, ω_{2k} are defined from an information point of view if the total number of data points, i.e. the product $N_1 N_2$ (recall that these are indexed beginning with zero) is greater than $3K$. In practice, though, one has to take into account noise, which effectively increases the rank of the signal subspace, and possible numerical limitations due to the highly nonlinear character of the HIP.

It is important to realize the difference between the present non-direct-product formulation of the 2D harmonic inversion problem, Eqn (20), and those proposed by others.[27–29] In the latter case the authors used models with a direct-product set of unknown spectral parameters, $\{\omega_{1k}, \omega_{2k'}, d_{kk'}\}$, $k = 1, 2, \ldots, K_1$, $k' = 1, 2, \ldots, K_2$ so that in the 2D plane the unknown spectral features would form a rectangular $K_1 \times K_2$ grid with total $K_1 + K_2 + K_1 K_2$ number of unknown parameters. In Eqn (20) the 2D frequencies ω_{1k}, ω_{2k} do *not* have to form a direct product 2D grid. Clearly, our non-direct-product model also allows a direct-product output (as, e.g., in the case of COSY and NOESY), while resulting in a much more compact representation for cases when the 2D spectra do not have direct-product patterns, e.g. HSQC or 2D-J spectra. These latter are expected to be the most suitable applications for the present technique.

Despite the long history of developing alternatives to the FT for 2D analysis, these alternatives are not commonly used in the practical analysis of typical spectra. Most likely, the reason is that applications of such methods require a great deal of human and computer time, they can be numerically unstable and can produce unreliable results, sensitive to the parameters of the fit and the signal-to-noise ratio. As such, the linear prediction (LP) method, which is often used in NMR, is rarely implemented for extracting the spectral parameters (ω_{1k}, ω_{2k}) and d_k as a 'line list' from real 2D NMR signals. Instead, after an FT in the F_2 dimension, it is typically implemented for 'extension' of 1D interferograms followed by their FT in this dimension.[12,13,27–29] On the other hand, if the spectral parameters (ω_{1k}, ω_{2k}) and d_k can be obtained then the spectrum can be constructed directly by summing over these parameters, avoiding any FT analysis. Thus, for a signal of suitable signal-to-noise ratio, and with a large number of points N_2 in t_2, it may be possible to generate a decent line list with a surprisingly small number of points N_1 in t_1. The small number of increments required, in turn, makes it possible to acquire more scans per increment than in the conventional 2D FT experiment. In some cases where, for example, an accurate chemical shift measurement is all that is required for input into a structural refinement program, FDM has enormous potential to speed up data throughput.

The results we show below are only preliminary. There is reason to believe that, with some further code development, FDM will deliver even better performance than that shown here.

APPLICATION OF FDM TO HSQC SPECTRA

Figure 3 shows a timing diagram for the particular PFG version of the HSQC experiment that we employed. The compensated PFG was used to achieve near zero linear phase correction in the carbon-13 dimension. As is well known, a 90° pulse leads to a mild linear phase roll with frequency which can be modeled by an instantaneous δ-function 90° pulse followed by a delay of length $1/\gamma B_1$. There are typically pre- and post-pulse delays for internal housekeeping and phase shifting, represented by the delays Δ. By setting the compensatory delay ε so that

$$\varepsilon = 4\Delta + \frac{2}{\gamma B_1} + \tau_{180} \quad (24)$$

where τ_{180} is the proton 180° pulse time (excluding any associated hardware delays), a very good approximation to the true $t_1 = 0$ signal can be obtained for the first increment, simplifying the phasing of the 2D spectrum. While a compensated PFG could be used for the decoding gradient G_1 there is little advantage for the HSQC sequence, as there is adequate time during the last $1/4J$ delay to apply a strong conventional PFG and still have adequate stabilization time. This hybrid approach keeps the suppression ratio extremely high,

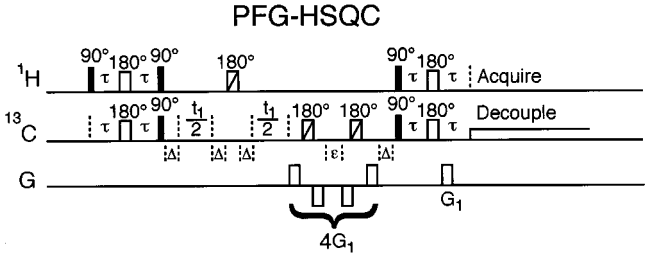

Figure 3. Pulse sequence timing diagram for the compensated PFG HSQC experiment. The scored icons are constant amplitude FM inversion pulses. On the carbon-13 channel these were 112 μs in duration using a 17.8 kHz RF field, whereas on the proton channel a 60 μs FM inversion pulse using a 25 kHz RF field was employed. With typical housekeeping delays $\Delta = 10$ μs on the proton and carbon-13 pulses and a 14 μs 90° pulsewidth on carbon-13, the compensating delay is $\varepsilon = 117.9$ μs.

while still giving a 2D data set with phase properties of exceptional fidelity.

Figure 4 shows the structure and proton NMR assignment of an aromatic molecule. The FT spectrum is nearly first order, and there is only very slight overlap between protons 9 and 5. The natural abundance HSQC 2D FT spectrum is contrasted with the 2D FDM ersatz spectrum in Fig. 5. In the upper panel a contour plot of the conventional 2D FT spectrum is shown. This data set was acquired with only four points in t_1 and 32 scans per increment and with separate data sets using first positive and then negative polarities for the decoding gradient, so that an absorption-mode 2D FT spectrum could be obtained. The spectrum was, of course, digitally filtered and extensively zero-filled before contouring. The lower panel is the 2D FDM ersatz spectrum obtained using only half the data (the negative polarity gradients) used for the top panel. There is clearly a substantial improvement in the resolution in the F_1 dimension, so that the carbon-13 shifts can be determined more easily; the experiment time is also halved. Compared with the 2D FT spectrum for a given experiment time, FDM thus gives us the enviable choice of acquiring either twice as many t_1 increments or twice as many scans per increment. Either option will result in a far superior spectral representation.

Perhaps even more telling is the comparison in Fig. 6. The top panel is the contour plot of the 2D FT spectrum of the same molecule used in Fig. 5 but now using eight points in t_1, and with a separate gradient set for each increment, to obtain the absorption-mode 2D spectrum. The lower panel shows the 2D FDM ersatz

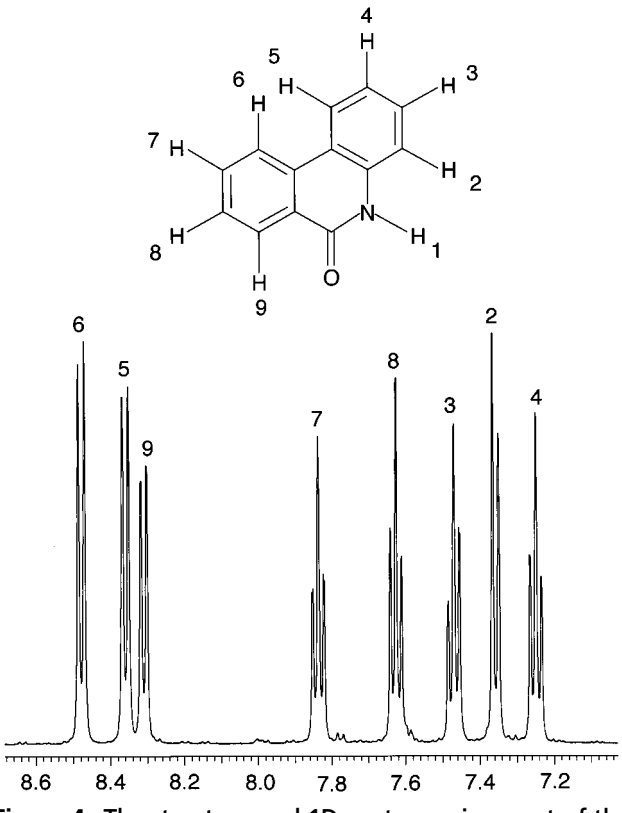

Figure 4. The structure and 1D proton assignment of the FT spectrum of the aromatic molecule 6(5*H*)-phenanthridinone in DMSO-d_6. The proton spectrum is well resolved and easy to assign.

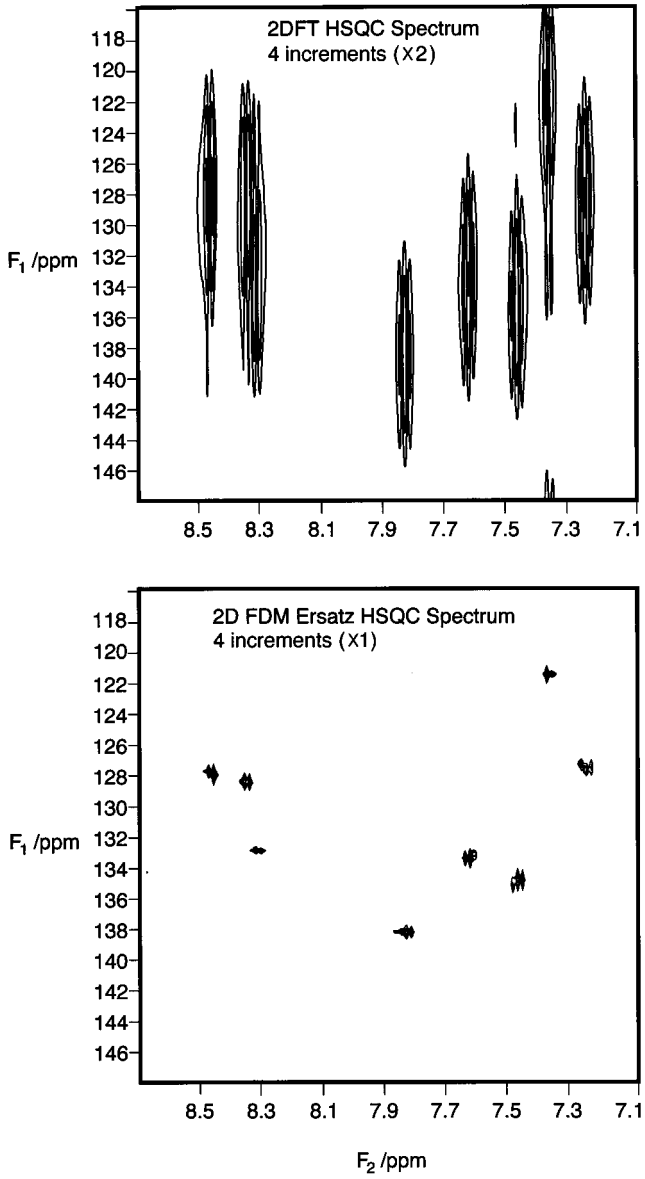

Figure 5. A comparison of the phase-sensitive 2D spectra of the aromatic molecule shown in Fig. 4 obtained with the pulse sequence of Fig. 3. The spectral width in F_2 was 1500 Hz and 1024 complex points were acquired for each FID. The spectral width in F_1 was 4000 Hz. The top contour plot is obtained from the 2D FT spectrum obtained with four t_1 increments in which the last gradient of Fig. 3 is applied with positive polarity, and for otherwise identical increments with negative polarity. The data have been apodized to avoid large truncation effects, and zero-filled in F_1 before Fourier transformation in this dimension, to give a smoother contour plot. The bottom spectrum is the FDM ersatz spectrum using four increments, and using only the first 300 complex points t_2 of each FID. It is constructed directly from the line list produced by FDM using Eqn (21). As there is no need to combine N- and P-type spectra in FDM, only half of the data, obtained with the negative polarity gradient, were used to obtain this result.

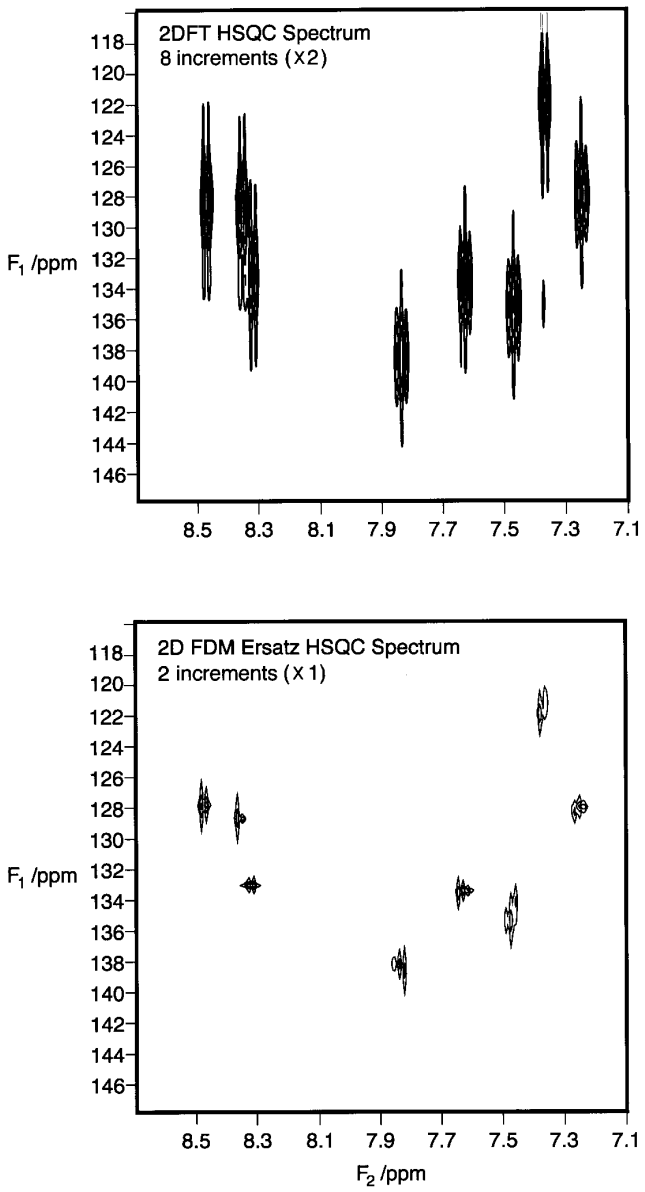

Figure 6. HSQC spectra obtained with the conditions listed in the caption to Fig. 5. Top: phase-sensitive 2D FT spectrum using eight points in t_1. Bottom: ersatz FDM spectrum using only two points in t_1. There is larger scatter in the F_1 peak positions, but the carbon-13 shifts can still be determined to within *ca.* 2 ppm and the distinct signals from each C–H pair are easy to pick out.

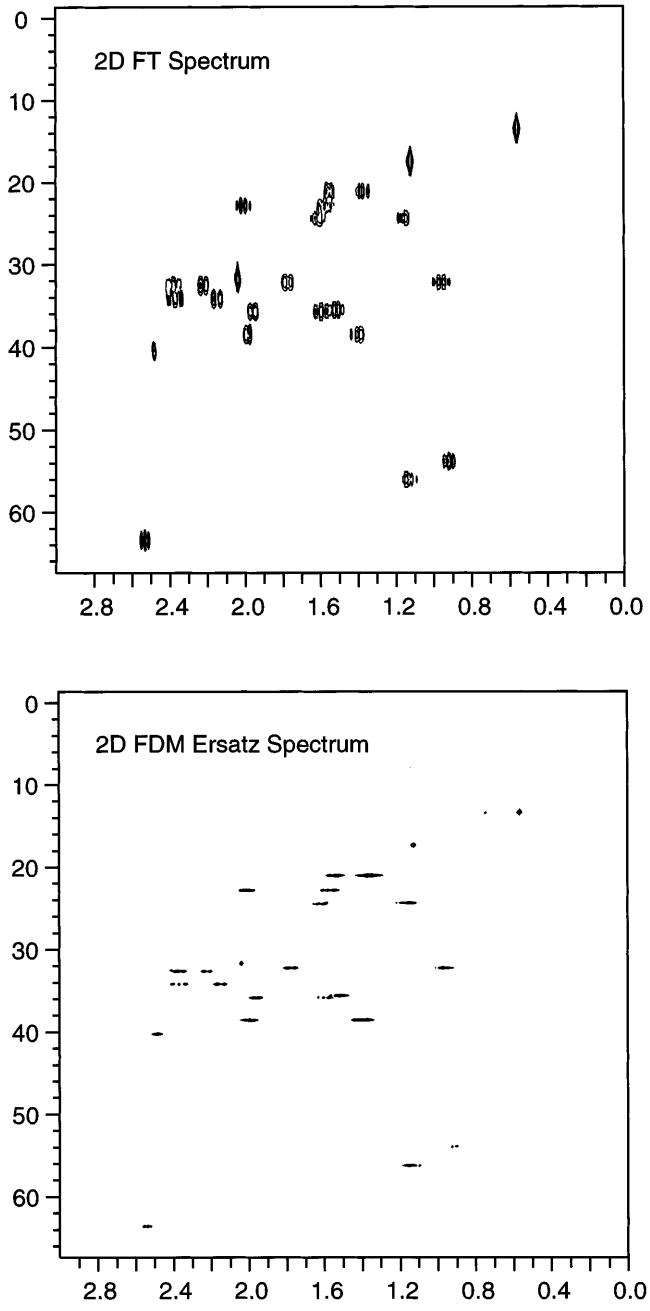

Figure 7. HSQC spectra of progesterone. Top: 2D FT spectrum obtained with 64 points in t_1 over a spectral width of 8250 Hz (66 ppm), zero filled to 256 points before Fourier transformation, and 2048 in t_2 over a spectral width of 2000 Hz. Bottom: 2D FDM ersatz spectrum obtained using the same 64 points in t_1 and using only the first 400 points of each FID in t_2, using the spectral representation of Eqn (22). The apparent resolution in F_2 is similar in the two spectra, but the resolution in F_1 is markedly superior in the FDM ersatz spectrum.

spectrum using only a single t_1 increment of 250 μs! A total of 32 scans were taken for each of the two values $t_1 = 0$ and $t_1 = 250$ μs. Aside from being eight times quicker to obtain than the 2D FT plot, the resolution in F_1 is still markedly superior. (The FFT spectrum obtained with only two t_1 points was not interpretable.) This example shows how an integrated 2D linear algebraic approach like 2D FDM is able to 'lock on' to spectral features in the 2D plane, even when a 1D LP approach in the F_1 dimension would be of questionable reliability. Once the F_2 dimension is processed with a Fourier transform, each t_1 interferogram is treated completely independently by the usual 1D analysis: if two Lorentzians partially overlap in F_2, frequency coordinates between the two peaks will necessarily contain two potentially different modulation frequencies, which would require at least four t_1 point to determine properly. In 2D FDM it is 2D features that are identified so that, in principle, all the points contributing to a Lorentzian feature in F_2 are used in concert to identify the F_1 frequency for that feature. By contrast, conventional LP methods have notable difficulties to process FIDs in

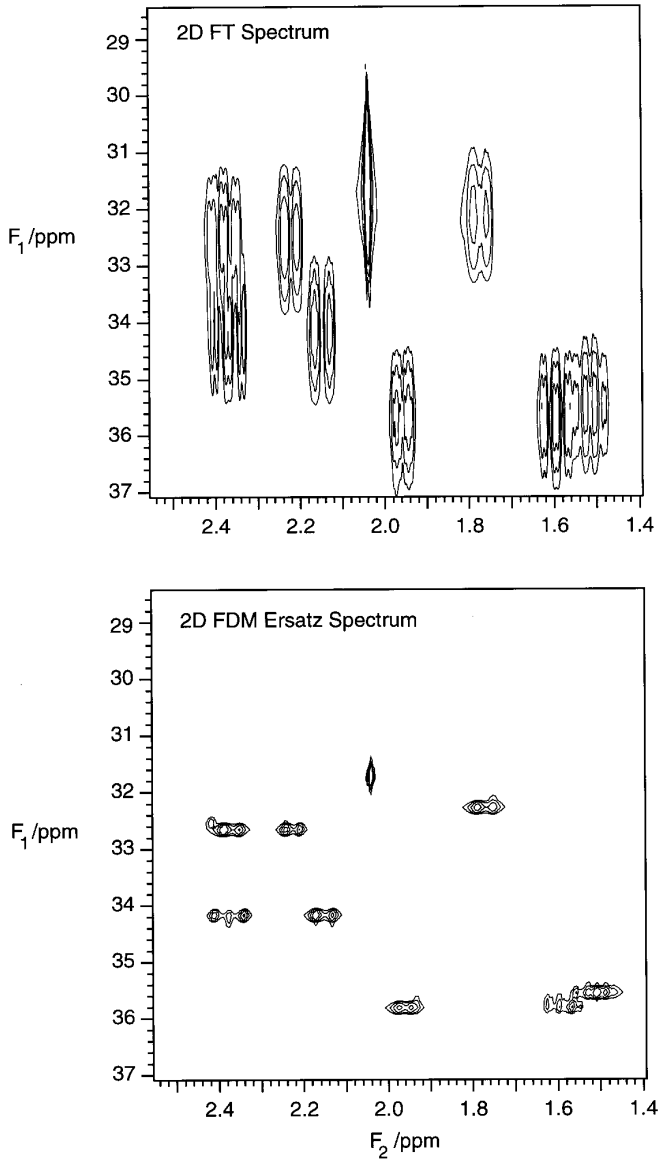

Figure 8. A small section of the 2D spectrum of Fig. 7 containing a strong methyl group signal and some weaker overlapping multiplets from non-equivalent methylene protons. Visual interpretation of the FDM ersatz spectrum is simpler to carry out. Note that the transform limited width in F_1 is >1 ppm under the conditions of the experiment.

F_2 if there are many time points N_2 and spectral features K because the size of the linear algebraic problem that is produced is huge, its solution involves ill-conditioned matrices and the unfavorable cubic scaling of the numerical effort means that the computation is exceedingly slow. Of course, complex spectra are exactly the case where multi-dimensional methods are most useful and most likely to be applied.

A case in point is shown in Fig. 7 for the 2D HSQC spectrum of the steroid progesterone, which has an extensively overlapped proton spectrum. A total of 64 t_1 increments were obtained, with two data sets using, respectively, positive and negative polarity for the decode gradient, as before. The phase-sensitive 2D FT spectrum is shown in the top panel and an ersatz 2D FDM spectrum (using only the negative polarity gradient data set) is shown in the bottom panel. The carbon-13 chemical shifts have been determined very accurately, and inequivalent methylene protons can be assigned by inspection. The narrowness of the peaks in F_1 makes them difficult to contour. Figure 8 shows an expansion of a small congested region for comparison. The improvement is more than cosmetic; the data acquisition can be done in half the time.

CONCLUSION

Pulsed field gradient techniques have well known advantages when it comes to suppressing undesired signals, especially when the latter are strong. Using coherence transfer pathway selection, clean phase modulated data sets can be obtained, and the use of the composite PFGs minimizes unwanted delays which would lead to phase rolls in the F_1 dimension, including those due to the finite width 90° pulses. These data sets are free of subtraction artifacts that would be present in a phase cycled HSQC experiment, and are suitable for direct extraction of spectral parameters using linear algebraic methods such as FDM.

We have shown FDM to be a powerful and efficient method of spectral parameter estimation. With sufficient sensitivity, it is possible to assign the protonated carbon-13 chemical shifts of simple molecules with just two proton spectra. While we have compared the ersatz FDM spectrum with the FT spectrum for the sake of familiarity, one should really attempt to compare the line list generated by first computing the FT spectrum and then using any smart peak picking algorithm, including the time for the latter algorithm in the total computational effort for obtaining a line list from the 2D time signal. In this case FDM will appear particularly advantageous.

More generally, we view FDM as a powerful adjunct to conventional FT analysis. It is possible to apply FDM to just small 'tough' spectral regions, where there is some question. The computation time for 2D FDM is only *ca.* 1 min on a low-end workstation and so it could, therefore, be carried out on-line as the experiment progresses. As more increments and/or scans are obtained, the features in the line list will be obtained with increasing fidelity. Once features in the line list are stable, the experiment can be terminated under computer control.

Acknowledgements

This material is based on work partially supported by a Dreyfus Foundation Teacher–Scholar Award and by the National Science Foundation, CHE-9625674. We are indebted to Professor Benny Gerber for the use of an SGI workstation.

REFERENCES

1. R. R. Ernst, G. Bodenhausen and A. Wokaun, *Principles of Nuclear Magnetic Resonance in One and Two Dimensions.* Clarendon Press, Oxford (1987).
2. G. Bodenhausen, H. Kogler and R. R. Ernst, *J. Magn. Reson.* **58**, 370 (1984).

3. P. B. Barker and R. Freeman, *J. Magn. Reson.* **64**, 334 (1985).
4. R. E. Hurd, *J. Magn. Reson.* **87**, 422 (1990).
5. D. J. States, R. A. Haberkorn and D. J. Ruben, *J. Magn. Reson.* **48**, 286 (1982).
6. G. Bodenhausen, R. Freeman, R. Niedermeyer and D. L. Turner, *J. Magn Reson.* **26**, 133 (1977).
7. W. P. Aue, J. Karhan and R. R. Ernst, *J. Chem. Phys.* **64**, 4226 (1976).
8. G. Bodenhausen and D. J. Ruben, *Chem. Phys. Lett.* **69**, 185 (1980).
9. J. Tang and J. R. Norris, *J. Chem. Phys.* **84**, 5210 (1986).
10. D. S. Stephenson, *Prog. Nucl. Magn. Reson. Spectrosc.* **20**, 515 (1988).
11. G. Zhu and A. Bax, *J. Magn. Reson.* **90**, 405 (1990).
12. R. de Beer and D. van Ormondt, in *NMR Basic Principles and Progress* Vol. 26, p. 201 (1992).
13. J. C. Hoch and A. S. Stern, *NMR Data Processing*. Wiley–Liss, New York (1996).
14. G. Wider, V. Dötsch and K. Wüthrich, *J. Magn. Reson. A* **108**, 255 (1994).
15. D. H. Wu and C. S. Johnson, *J. Magn. Reson. A* **110**, 113 (1994).
16. T. J. Hwang and A. J. Shaka, *J. Magn. Reson. A* **112**, 275 (1995).
17. H. Hu and A. J. Shaka, *J. Magn. Reson.* submitted for publication.
18. J. Baum, R. Tycko and A. Pines, *Phys. Rev. A* **32**, 3435 (1985).
19. M. R. Wall and D. Neuhauser, *J. Chem. Phys.* **102**, 8011 (1995).
20. V. A. Mandelshtam and H. S. Taylor, *Phys. Rev. Lett.* **78**, 3274 (1997).
21. V. A. Mandelshtam and H. S. Taylor, *J. Chem. Phys.* **107**, 6756 (1997).
22. V. A. Mandelshtam and H. S. Taylor, *J. Chem. Phys.* (accepted).
23. V. A. Mandelshtam, H. S. Taylor and A. J. Shaka, *J. Magn. Reson.* submitted for publication.
24. S. Marple, Jr. *Digital Spectral Analysis with Applications.* Prentice-Hall, Englewood Cliffs, NJ (1987).
25. R. Roy, B. G. Sumpter, G. A. Pfeffer, S. K. Gray and D. W. Noid, *Comput. Phys. Rep.* **205**, 109 (1991).
26. J. Tang and J. Norris, *J. Magn. Reson.* **79** 190 (1988).
27. G. Zhu and A. Bax, *J. Magn. Reson.* **98**, 192 (1992).
28. H. Gesmar and J. J. Led, *J. Magn. Reson.* **83**, 53 (1989).
29. H. Gesmar and J. J. Led, in *Computational Aspects of the Study of Biological Macromolecules by Nuclear Magnetic Resonance spectroscopy*, edited by J. C. Hoch, F. M. Poulson and C. Redfield, pp. 67–85. Plenum Press, New York (1991).

APPENDIX

FDM for harmonic inversion of two-dimensional signals

For a 2D complex time signal c_{n_1,n_2} the 2D generalization of Eqn (6) is given in Eqn (20), which can be identified with the plane wave representation of a 2D array. To simplify the following equations, we adopt dimensionless time units $\tau_1 = \tau_2 = 1$ for the sampling intervals in the 2D experiment, which is equivalent to replacing $\tau_1\omega_{1k}$ by ω_{1k} and $\tau_2\omega_{2k}$ by ω_{2k}. The key ansatz of 2D FDM is obtained by introducing two commuting complex symmetric operators $\hat{\Omega}_1$, $\hat{\Omega}_2$, having the same set of eigenvectors $\mathscr{Y}_k$ but different eigenvalues ω_{1k} and ω_{2k} which are the unknown complex frequencies:

$$c_{n_1,n_2} = (\Phi_0 | \exp(-in_1\hat{\Omega}_1)\exp(-in_2\hat{\Omega}_2)\Phi_0) \quad \text{(A1)}$$

As in the 1D case, the set of eigenvectors $\mathscr{Y}_k$ and the 'initial state' Φ_0 are defined implicitly by $d_k = (\mathscr{Y}_k | \Phi_0)^2$. We are interested in extracting the complex frequencies $(\omega_{1k}, \omega_{2k})$ in a small 2D frequency domain,

$$2\pi \text{ Re } \{(\omega_{1k}, \omega_{2k})\} \in \mathscr{D}_f = [f_{1\min}, f_{1\max}] \times [f_{2\min}, f_{2\max}]$$

of the F_1F_2 plane. The 2D Fourier basis is consequently defined by introducing a small grid $2\pi\boldsymbol{\varphi}_j \equiv 2\pi(\varphi_{1j}, \varphi_{2j}) \in \mathscr{D}_f, j = 1, 2, \ldots, K_{\text{win}}$:

$$\Psi(\boldsymbol{\varphi}) \equiv \Psi(\varphi_1, \varphi_2) = \sum_{n_1=0}^{M_1} \exp[in_1(\varphi_1 - \hat{\Omega}_1)] \times \sum_{n_2=0}^{M_2} \exp[in_2(\varphi_2 - \hat{\Omega}_2)]\Phi_0 \quad \text{(A2)}$$

The matrix elements $U^{(\boldsymbol{p})}_{jj'} \equiv U^{(\boldsymbol{p})}(\boldsymbol{\varphi}_j, \boldsymbol{\varphi}_{j'})$ of the operator

$$\exp(-i\boldsymbol{p}\boldsymbol{\Omega}) \equiv \exp(-ip_1\hat{\Omega}_1)\exp(-ip_2\hat{\Omega}_2)$$

in this basis are given by

$$U^{\boldsymbol{p}}(\boldsymbol{\varphi}, \boldsymbol{\varphi}') \equiv (\Psi(\boldsymbol{\varphi})|\exp(-i\boldsymbol{p}\boldsymbol{\Omega})\Psi(\boldsymbol{\varphi}')) = \sum_{n_1'=0}^{M_1}\sum_{n_1=0}^{M_1}\sum_{n_2'=0}^{M_2}\sum_{n_2=0}^{M_2} \exp\{i[n_1(\varphi_1 - \varphi_1') + n_2(\varphi_2 - \varphi_2')]\} \times \exp\{i[\varphi_1'(n_1 + n_1') + \varphi_2'(n_2 + n_2')]\} \times c_{(n_1+n_1'+p_1),(n_2+n_2'+p_2)} \quad \text{(A3)}$$

By recognizing the same structure that occurs in the 1D case [see Eqn (11)], we finally obtain the simplified form

$$U^{(\boldsymbol{p})}(\boldsymbol{\varphi}, \boldsymbol{\varphi}') = \sum_{n_1=0}^{2M_1} S_{n_1}(\varphi_1, \varphi_1'; M_1) \times \sum_{n_2=0}^{2M_2} S_{n_2}(\varphi_2, \varphi_2'; M_2)c_{n_1+p_1,n_2+p_2} \quad \text{(A4)}$$

which is a 2D generalization of Eqn (12). The definition of S_n is given in Eqns (13) and (14).

The 2D analog for the 1D generalized eigenvalue problem reads

$$\mathbf{U}^{(\boldsymbol{p})}\mathbf{B}_k = \exp(-i\omega_{\boldsymbol{p}k})\mathbf{U}^{(0)}\mathbf{B}_k \quad \text{(A5)}$$

where $\omega_{\boldsymbol{p}k} = p_1\omega_{1k} + p_2\omega_{2k}$ and, as in the 1D case, the elements B_{jk} of the eigenvectors $\mathbf{B}_k$ define the relation beteen Y_k and Ψ_k according to

$$Y_k = \sum_{j=1}^{K_{\text{win}}} B_{jk}\Psi_j \quad \text{(A6)}$$

The amplitudes $d_k = (Y_k|\Phi_0)^2$ can be computed using the 2D analog of Eqn (18):

$$d_k^{1/2} = \frac{[1 - \exp(-\gamma_1)][1 - \exp(-\gamma_2)]}{(\{1 - \exp[-(M_1 + 1)\gamma_1]\} \times \{1 - \exp[-(M_2 + 1)\gamma_2]\})} \times \sum_{j=1}^{K_{\text{win}}} B_{jk}U^{(0)}(\boldsymbol{\varphi}_j, \boldsymbol{\omega}_k + i\boldsymbol{\gamma}_k) \quad \text{(A7)}$$

where $\boldsymbol{\omega}_k + i\boldsymbol{\gamma}_k \equiv (\omega_{1k} + i\gamma_1, \omega_{2k} + i\gamma_2)$. In the $\gamma_1 = \gamma_2 \to \infty$ limit, Eqn (A7) can be reduced to a simpler, but generally less accurate expression:

$$d_k^{1/2} = \sum_{j=1}^{K_{\text{win}}} B_{jk}\sum_{n_1=0}^{M_1}\sum_{n_2=0}^{M_2}\exp(in_1\varphi_{1j})\exp(in_2\varphi_{2j})c_{n_1,n_2} \quad \text{(A8)}$$

A comment should be made on how to identify the pairs of eigenvalues ω_{1k}, ω_{2k} which in principle come from two independent diagonalizations, for example using Eqn (A5) with $\boldsymbol{p} = (1, 0)$ and $\boldsymbol{p} = (0, 1)$, respectively. As theoretically the eigenvectors $\mathbf{B}_k$ resulting from the two diagonalizations have to be the same, one possible solution is to first solve Eqn (A5) for a particular projection $\boldsymbol{p} = (p_1, p_2)$ to obtain the eigenvectors $\mathbf{B}_k$ and then use the equation

$$\exp(-i\omega_{\boldsymbol{p}k}) = \frac{(\mathbf{B}_k \mid \mathbf{U}^{(\boldsymbol{p})}\mathbf{B}_k)}{(\mathbf{B}_k \mid \mathbf{U}^{(\mathbf{0})}\mathbf{B}_k)} \tag{A9}$$

with $\boldsymbol{p} = (1, 0)$ and $\boldsymbol{p} = (0, 1)$ to compute ω_{1k} and ω_{2k}, respectively. However, because of the noise present in the signal, the eigenvectors $\mathbf{B}_k$ for different projections $\boldsymbol{p}$ are not exactly the same [they are identical only when the assumption of Eqn (A1) is exact] and therefore the frequencies obtained *indirectly* using Eqn (A9) are always much less accurate than those computed *directly* as the eigenvalues of Eqn (A5). Because of this, we have developed a strategy which uses the two sets of frequencies $\{\omega_{1k}\}$ and $\{\omega_{2k}\}$ obtained in two independent diagonalizations with $\boldsymbol{p} = (1, 0)$ and $\boldsymbol{p} = (0, 1)$ and which are assigned (identified by comparing the corresponding eigenvectors $\mathbf{B}_k$. It should be noted that an even more sophisticated strategy can be adopted by employing more than two projections, e.g. $\boldsymbol{p} = (1, 0)$, (0, 1) and (1, 1), each of which results in a set of eigenvalues $\{\omega_{\boldsymbol{p}k}\}$ and eigenvectors $\mathbf{B}_k$. The frequency assignment can be done using the equation $\omega_{\boldsymbol{p}k} = p_1\,\omega_{1k} + p_2\,\omega_{2k}$.

With regard to the numerical effort of 2D FDM, note that inspection of Eqns (A4) and (18) shows that for an arbitrary choice for the 2D grid $\boldsymbol{\varphi}_j = (\varphi_{1j}, \varphi_{2j})$, $j = 1, 2, \ldots, K_{\text{win}}$, evaluation of all the matrix elements $U_{jj'}^{(\boldsymbol{p})}$ scales as $K_{\text{win}}^2 \times N_1 \times N_2$, i.e. linearly with respect to the number of elements in the 2D array c_{n_1,n_2}. If for $\boldsymbol{\varphi}_j$ we use a direct product grid $\boldsymbol{\varphi}_j = (\varphi_{j_1}, \varphi_{j_2})$ with $j_1 = 1, 2, \ldots, K_{1\text{win}}$ and $j_2 = 1, 2, \ldots, K_{2\text{win}}$ with $K_{\text{win}} = K_{1\text{win}} \times K_{2\text{win}}$, then the total numerical effort of evaluating $\mathbf{U}^{\boldsymbol{p}}$ can be further reduced to $K_{\text{win}} \times N_1 \times N_2$. Note that K_{win} is never a large number in these equations, whereas $N_1 \times N_2$ can be potentially very large.